JPEDAV (2006) 27:63-74
DOI: 10.1361/105497106X92826
1547-7037/$19.00 ©ASM International

Thermodynamic Study of the Phase Equilibria in the Sn–Ti–Zn Ternary System

K. Doi, S. Ono, H. Ohtani, and M. Hasebe

(Submitted January 4, 2005; in revised form March 17, 2005)

The Sn-Ti-Zn ternary phase diagram has been constructed using the CALPHAD technique. The Ti-Zn binary system phase boundaries were determined using differential scanning calorimetry and the solid-liquid diffusion couples method. In addition, the formation energy of some stoichiometric compounds was obtained using first-principle band energy calculations. For the ternary system, some alloys were prepared by equilibration at 600 or 700 °C, and the compositions of the precipitates were analyzed using electron probe microanalysis. Thermodynamic assessment of the Ti-Zn and Sn-Ti-Zn systems was performed based on the experimental information and by adopting reported values of the thermodynamic properties of the Sn-Zn and Sn-Ti binary systems. Microstructural observation showed that $Sn_3Ti_5Zn_{12}$ exists in the ternary system. Seven types of invariant reaction on the Sn-rich liquidus surface of the ternary system are predicted by the phase diagram calculations. The ternary eutectic point falls at 0.0009 mass% Ti and 8.69 mass% Zn, at T = 192.40 °C, which is slightly lower than the calculated eutectic point of Sn-Zn binary alloy (T= 192.41 °C). Based on these results, a nonequilibrium solidification process using the Scheil model was simulated.

Keywords lead-free solders, liquidus surface, phase diagram, surface tension, thermodynamic analysis

1. Introduction

The Pb-Sn eutectic alloy is widely used as a solder in high-density mountings in electronic devices. The wettability and the connectivity of this alloy are excellent, and its melting point is low. Thus, any thermal effect on an electronic device from this material is confined to a small area. However, the toxicity of the lead in this alloy is commonly known. In particular, lead leaching into underground water from waste electronic devices can lead to significant harmful effects on humans and on the environment. The development of lead-free solder materials is, therefore, of high importance to the electronics industry.[1]

Sn-Ag-Cu alloy has been used as a Pb-free solder, but it has a melting point of 218 °C, which is considerably higher than the 183 °C of conventional Pb-Sn eutectic alloy. Because of this, problems arise with workability during the reflow process when the heat resistivity of the electronic device does not change correspondingly. Zinc is an important additive to Sn-based solder alloys because Zn alloying lowers their melting point, although the wettability deteriorates and oxidation is accelerated by the addition of Zn. The eutectic point of Sn-Zn binary alloy is close to that of Pb-Sn solders. Thus, changes in conventional processing may not be necessary on substituting Sn-Zn-based solders. Moreover, due to the lower melting temperature, thermal damage to electronic devices would be restricted to a limited region. Therefore, Sn-Zn alloys are promising candidates for a Pb-free solder. The addition of Ti to this alloy could possibly promote the precipitation of Ti-Zn based intermetallic compounds, which would improve the mechanical properties of the alloy.

Therefore, we have carried out a thermodynamic analysis of the Sn-Ti-Zn ternary system based on experimental results obtained by electron probe microanalysis (EPMA) measurements and differential scanning calorimetry (DSC) analysis.

2. Procedures

2.1 Measurement of the Phase Boundaries in the Ti-Zn Binary System

The phase boundaries of the Ti-Zn binary system were experimentally determined using the solid-liquid diffusion couples and DSC methods. The samples were prepared by inserting pure granular Zn (99.99%) in a 5 mm diameter hole that had been drilled into a column of pure Ti (99.9%, diameter = 8 mm and height = 15 mm), as shown in Fig. 1. The surface of the samples was subjected to a chemical polish using a hydrogen peroxide:hydrofluoric acid:water mixture (90:7:3). A pure Ti lid was placed on the sample to avoid loss of Zn through volatilization. The diffusion

This paper was presented at the International Symposium on User Aspects of Phase Diagrams, Materials Solutions Conference and Exposition, Columbus, Ohio, 18-20 October, 2004.

K. Doi, Graduate School, Kyushu Institute of Technology, Kitakyushu 804-8550, Japan; **S. Ono,** Graduate School, Kyushu Institute of Technology, Kitakyushu 804-8550, Japan, and present address: Fujitsu System Solutions Co. Ltd, Tokyo 113-0021, Japan; and **H. Ohtani,** and **M. Hasebe,** Department of Materials Science and Engineering, Kyushu Institute of Technology, Kitakyushu 804-8550, Japan, CREST, Japan Science and Technology Agency. Contact e-mail: ohtani@matsc.kyutech.ac.jp.

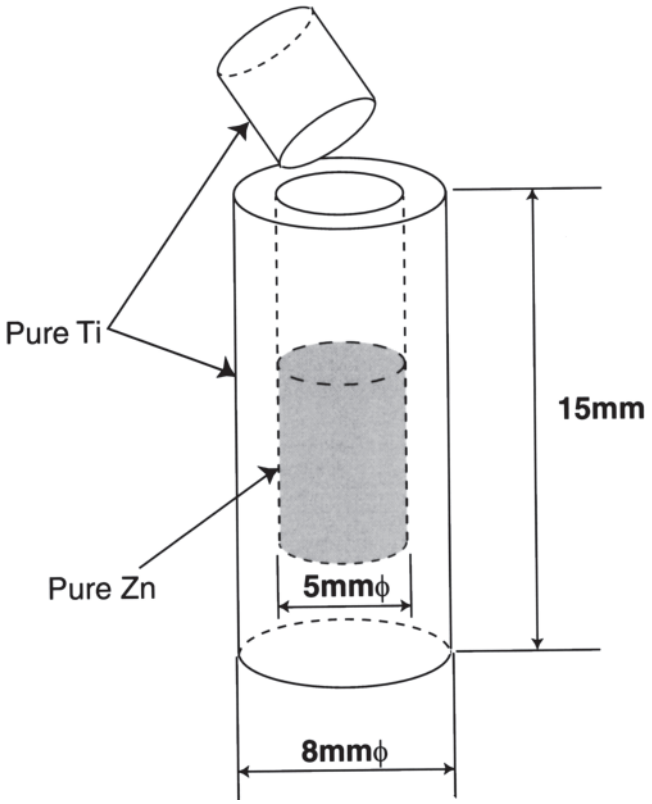

Fig. 1 Configuration of the solid-liquid diffusion couples

couples were sealed in transparent quartz capsules under pure argon gas, and these were heated for 120 h at temperatures of 700, 800, 1000, and 1100 °C in the equilibrium experiments. After quenching in iced brine, the specimens were cut parallel to the direction of diffusion, and the concentration profile of each constituent across the solid/liquid interphase boundary was determined using a Jeol (Chiba-City, Chiba) JCXA-733 electron probe microanalyzer.

On the other hand, the alloy used in the DSC measurements was in the Zn-rich region of the Ti-Zn binary system and was prepared from pure granular Zn (99.99%) wrapped in 0.005 mm thick Ti foil (99.6%). The samples were enclosed in silica tubes and homogenized at a temperature of about 770 °C. The composition of the resulting alloy was 5 mass% Ti. After quenching the samples in iced brine, thermal analysis was carried out using a Seiko Instruments (Tokyo, Japan) Exstar 6000 differential scanning calorimeter. Alumina was used as the standard material, and the measurements were performed under an argon atmosphere. The sample heating and cooling rates were set to 3 °C/min. The experimental results are shown in Table 1, where the peak temperature values during heating are shown, considering any experimental error incurred by supercooling.

2.2 Measurement of the Phase Boundaries of the Sn-Ti-Zn Ternary System

The phase boundaries of the Sn-Ti-Zn ternary system were measured using DSC in the three sections: 3 mass% Ti, 10 mass% Ti, and 10 mass% Zn. The alloys for the DSC measurements were prepared from Sn (99.99%), Ti (99.9%), and Zn (99.99%). The alloys were prepared by enclosing each of the pure metals in proportions at the desired alloy composition in a silica tube and then homogenizing the metals at a temperature of about 800 °C. After quenching the specimens in iced brine, thermal analysis was carried out using the same procedure described above. The experimental results are shown in Table 1, where the peak temperatures in the heating processes are also listed.

2.3 Analysis of the Microstructure of the Sn-Ti-Zn Ternary Alloys

The equilibrated Sn-Ti-Zn ternary alloys were observed using microscopy. The alloy was prepared by enclosing the pure metals in a silica tube in the target composition as listed in Table 2, and these were then heated to 600 or 700 °C and maintained at that temperature for 72 h. After equilibration, the specimen was quenched in iced brine. The specimen was etched using dilute hydrochloric acid solution, and the microstructure was observed using an optical microscope. The compositions of the precipitates were analyzed using EPMA. Some scatter was observed in the analyzed liquid phase compositions, which was attributed to solidification structures, and thus, the experimental data were used as the reference values. The solid phases were very uniform in composition.

2.4 Thermodynamic Modeling of the Solution Phases

2.4.1 Liquid (L) and Primary Solution Phases. The regular solution approximation was applied to the liquid phase. The molar Gibbs energy G_m^L was calculated using the following equation:

$$G_m^L = x_{Sn}\,{}^oG_{Sn}^L + x_{Ti}\,{}^oG_{Ti}^L + x_{Zn}\,{}^oG_{Zn}^L + RT(x_{Sn}\ln x_{Sn} + x_{Ti}\ln x_{Ti} + x_{Zn}\ln x_{Zn}) + x_{Sn}x_{Ti}L_{Sn,Ti}^L + x_{Sn}x_{Zn}L_{Sn,Zn}^L + x_{Ti}x_{Zn}L_{Ti,Zn}^L + x_{Sn}x_{Ti}x_{Zn}L_{Sn,Ti,Zn}^L \quad \text{(Eq 1)}$$

where ${}^oG_i^L$ denotes the molar Gibbs energy of element i in the liquid state. This quantity is called the lattice stability parameter, and is described by the formula[2]:

$${}^oG_i^\phi - {}^oH_i^{ref} = A + BT + CT\ln T + DT^2 + ET^3 + FT^7 + IT^{-1} + JT^{-9} \quad \text{(Eq 2)}$$

where ${}^oH_i^{ref}$ denotes the molar enthalpy of the pure element i in its stable state at $T = 25$ °C. The parameter $L_{i,j}^L$ denotes the interaction energy between i and j in the liquid phase and has a compositional dependency following the Redlich-Kister polynomial[3]:

$$L_{i,j}^L = {}^0L_{i,j}^L + {}^1L_{i,j}^L(x_i - x_j) + {}^2L_{i,j}^L(x_i - x_j)^2 + \ldots + {}^nL_{i,j}^L(x_i - x_j)^n \quad \text{(Eq 3)}$$

where

$${}^nL_{i,j}^L = a + bT + cT\ln T + dT^2 + \ldots \quad \text{(Eq 4)}$$

Table 1 Experimental phase boundaries of the Sn-Ti-Zn system determined by DSC

System	Alloy composition, mass%			Peak temperature, °C				
Ti-Zn		Ti	Zn					
		3.0	97.0		411.2	458.7	621.2	
Sn-Ti-Zn	**Sn**	**Ti**	**Zn**					
10 mass% Zn series	88.0	2.0	10.0	198.4	222.6	633.7	…	…
	86.0	4.0	10.0	198.4	225.4	665.2	…	…
	84.0	6.0	10.0	198.2	231.5	651.9	730.5	…
	82.0	8.0	10.0	197.9	235.9	771.2	…	…
3 mass% Ti series	77.0	3.0	20.0	197.9	280.0	493.6	596.8	…
	57.0	3.0	40.0	197.7	343.8	620.9	700.6	…
	37.0	3.0	60.0	197.9	366.0	609.0	652.8	…
	17.0	3.0	80.0	197.7	369.7	544.7	638.8	674.1
10 mass% Ti series	70.0	10.0	20.0	197.8	561.4	691.9	…	…
	50.0	10.0	40.0	197.8	337.7	652.7	724.6	758.2
	30.0	10.0	60.0	197.9	369.1	778.2	…	…
	10.0	10.0	80.0	414.0	509.9	665.2	689.5	…

Table 2 Experimental solid compositions of samples equilibrated at 600 and 700 °C

Temperature, °C	Specimen No.	Alloy composition, mass%			Phase	Composition of phase, mass%		
		Sn	Ti	Zn		Sn	Ti	Zn
600	E6-1	70	10	20	Sn_5Ti_6	62.14	31.65	4.29
					Liquid	70.93	1.06	30.01
	E6-2	60	10	30	Sn_5Ti_6	60.61	34.11	4.91
					Liquid	57.08	1.17	41.75
	E6-3	50	10	40	Sn_5Ti_6	60.32	33.36	5.59
					Liquid	57.61	1.20	41.19
					$Sn_3Ti_5Zn_{12}$	27.82	17.61	54.88
	E6-4	40	10	50	Liquid	57.81	1.02	41.17
					$Sn_3Ti_5Zn_{12}$	28.58	17.33	54.64
	E6-5	30	10	60	Liquid	37.81	0.11	62.09
					$Sn_3Ti_5Zn_{12}$	27.55	17.87	55.52
700	E7-1	20	8	62	Liquid	22.51	6.51	65.35
					$Sn_3Ti_5Zn_{12}$	25.52	17.75	57.82
	E7-2	16	9	75	Liquid	1.04	0.16	98.8
					$Sn_3Ti_5Zn_{12}$	22.77	18.37	60.97
	E7-3	13	12	75	Liquid	0.29	0.86	98.85
					$Sn_3Ti_5Zn_{12}$	18.43	18.89	65.47
					Zn_3Ti	0.31	16.92	79.51

The term $L^{L}_{Sn,Ti,Zn}$ is the ternary interaction parameter between elements Sn, Ti, and Zn. The composition dependency of the interaction parameters is expressed:

$$L^{L}_{Sn,Ti,Zn} = x_{Sn}{}^{1}L^{L}_{Sn,Ti,Zn} + x_{Ti}{}^{2}L^{L}_{Sn,Ti,Zn} + x_{Zn}{}^{3}L^{L}_{Sn,Ti,Zn} \quad \text{(Eq 5)}$$

The Gibbs energies of the Sn-rich bct phase (βSn), the Zn-rich hcp phase (Zn), and the Ti-rich hcp and bcc phases (α and βTi, respectively) were also described using Eq 1. The Gibbs energy of Sn-rich diamond phase (αSn) was also described as pure substance.

2.4.2 $SnTi_3$ Phase. The $SnTi_3$ phase formed in the Sn-Ti system has a hexagonal close-packed (hcp)-based $D0_{19}$ ordered structure, with a narrow homogeneity range at high temperatures. The chemical formula of this phase was considered to be $(Sn,Ti)(Sn,Ti)_3$,[4] and the free energy was described by the two-sublattice model:

$$\begin{aligned} G_m^{SnTi_3} = {} & y^{I}_{Sn}y^{II}_{Sn}{}^{\circ}G^{SnTi_3}_{Sn:Sn} + y^{I}_{Sn}y^{II}_{Ti}{}^{\circ}G^{SnTi_3}_{Sn:Ti} + y^{I}_{Ti}y^{II}_{Sn}{}^{\circ}G^{SnTi_3}_{Ti:Sn} \\ & + y^{I}_{Ti}y^{II}_{Ti}{}^{\circ}G^{SnTi_3}_{Ti:Ti} + RT(y^{I}_{Sn}\ln y^{I}_{Sn} + y^{I}_{Ti}\ln y^{I}_{Ti}) \\ & + 3RT(y^{II}_{Sn}\ln y^{II}_{Sn} + y^{II}_{Ti}\ln y^{II}_{Ti}) + y^{I}_{Sn}y^{II}_{Sn}y^{II}_{Ti}L^{SnTi_3}_{Sn:Sn,Ti} \\ & + y^{I}_{Ti}y^{II}_{Sn}y^{II}_{Ti}L^{SnTi_3}_{Ti:Sn,Ti} + y^{I}_{Sn}y^{I}_{Ti}y^{II}_{Sn}L^{SnTi_3}_{Sn,Ti:Sn} \\ & + y^{I}_{Sn}y^{I}_{Ti}y^{II}_{Ti}L^{SnTi_3}_{Sn,Ti:Ti} \end{aligned} \quad \text{(Eq 6)}$$

where, for example, ${}^{\circ}G^{SnTi_3}_{Sn:Ti}$ represents the free energy of a compound Sn_1Ti_3 when sublattices I and II are occupied by Sn atoms and Ti atoms, respectively. The term y_i^S denotes the site fraction of element *i* in sublattice *S*. The parameter $L^{SnTi_3}_{i,j:k}$, for example, denotes the interaction energy between unlike atoms on the first sublattice, when the second sublattice sites are occupied by k atoms.

2.4.3 Intermetallic Line Compounds. The binary intermetallic compound phases with zero homogeneity range, i.e., Sn_5Ti_6, Sn_3Ti_5, $SnTi_2$, $TiZn_{15}$, $TiZn_{10}$, $TiZn_5$, $TiZn_3$, $TiZn_2$, TiZn, and Ti_2Zn, were treated as being stoichiometric compounds. The Gibbs energy of the $TiZn_2$ phase, for example, is expressed by the following equation, adopting the stable structure for the elements as the thermodynamic standard state:

$${}^{o}G^{TiZn_2}_{Ti:Zn} - {}^{o}G^{hcp}_{Ti} - 2 \cdot {}^{o}G^{hcp}_{Zn} = a + bT + cT\ln T + dT^2 \quad \text{(Eq 7)}$$

The $Sn_3Ti_5Zn_{12}$ ternary phase will be discussed later, but this phase was also treated as a stoichiometric compound.

2.5 First-Principle Calculations for Intermetallic Phases

There is little information on the thermodynamic properties of the Ti-Zn binary system. Therefore, to supplement this lack of data, the enthalpies of formation for the $TiZn_3$ phase with a $L1_2$ structure and the TiZn phase with a B2 structure were obtained using the Full Potential Linearized Augmented Plane Wave (FLAPW) method. The FLAPW method, as embodied in the WIEN2k software package,[5] is one of the most accurate schemes for electronic calculations, allowing for precise calculations of the total energies in a solid. This package was therefore used in our energetic calculations. The FLAPW method uses a scheme to solve many electron problems based on the local spin density approximation (LSDA) approach. In this framework, the unit cell is divided into two regions: nonoverlapping atomic spheres and an interstitial region. Inside the atomic spheres, the wavefunctions of the valence states are expanded by linear combination of the radial functions and spherical harmonics, while a plane wave expansion is used in the interstitial region. Because the LSDA approach includes an approximation for both the exchange and correlation energies, it has been recently expanded on, by adding gradient terms for the electron density to the exchange-correlation energy. This has led to the generalized gradient approximation (GGA) method suggested by Perdew et al.,[6] and the present work used this improved method over the conventional LSDA approach.

In the present computations, Muffin-tin radii of 2.0 au (0.106 nm) for Ti and Zn were assumed. The value of RK_{max} was fixed at 9.0, which almost corresponds to the 20 Ry (270 eV) cut-off energy used in this work.

3. Results and Discussion

3.1 Thermodynamic Description of the Binary Systems

A brief outline of thermodynamic analysis of each binary system will be summarized in this section. The descriptions of the lattice stability parameters for each pure element were obtained mainly from the Scientific Group Thermodata Europe (SGTE) data[2] and are shown in Table 3.

3.1.1 Sn-Zn Binary System. The Sn-Zn binary system is a simple eutectic-type phase diagram, composed of liquid, α and βSn, and Zn solutions. The adopted thermodynamic description[7] is shown in Table 4, and the binary phase diagram is illustrated in Fig. 2(a). The gas phase was treated as an ideal mixture of Sn, Sn_2, and Zn in the calculation.

3.1.2 Sn-Ti Binary System. There are ten phases in the Sn-Ti system: liquid, α and βSn, α and βTi, ordered hexagonal $SnTi_3$ with the $D0_{19}$ structure, $SnTi_2$ with the $B8_2$ structure, Sn_3Ti_5 with the $D8_8$ structure, and the high- and low-temperature forms of Sn_5Ti_6,[4,8] in the thermodynamic description of this binary system, although a polymorphic transformation of Sn_5Ti_6 was excluded from the present thermodynamic analysis. In the current study, the thermodynamic description used is shown in Table 4, and the calculated binary phase diagram is illustrated in Fig. 2(b).

3.1.3 Ti-Zn Binary System. Only partial phase equilibria of the Ti-Zn binary system was deduced, owing to the large difference between the high melting temperature of Ti (1670 °C) and the low boiling point of Zn (907 °C). Several intermetallic compounds have been found in this system; however, the phase relationships are still obscure except in the extreme Zn-rich region. The solubility of Zn in α and βTi or the effect of Zn on the transformation temperature is unknown.[8] Recently, Vassilev et al.[9,10] investigated the Zn-rich region of the phase diagram using diffusion couples, differential scanning calorimetry, and x-ray diffraction. However, the annealing times used, e.g., 1800 and 3600 s at 700 °C, seems too short to obtain the true equilibrium state.

A typical example of the concentration profile in a solid-liquid diffusion couple obtained in the current study is shown in Fig. 3, indicating seven types of interphase boundary in the sample. According to the EPMA analysis, the formation of $TiZn_3$, $TiZn_2$, TiZn, and Ti_2Zn can be observed sequentially on passing from the left-hand side to the right-hand side of the concentration profile in Fig. 3. The $TiZn_{15}$, $TiZn_{10}$, and $TiZn_5$ phases were not observed in the diffusion couple at the temperatures studied. The three compositional gaps on the right-hand side of the profile in Fig. 3 may correspond to the phase boundaries of the α and βTi. According to the present experimental results, Murray's peritectic reaction, $L + TiZn_2 \leftrightarrow TiZn_3$ occurring at 650 °C,[8] was not observed. In a similar manner, interphase boundaries of $TiZn_3$, $TiZn_2$, and TiZn, as well as the primary Ti solid solution interphase boundary, were observed in the diffusion couple equilibrated at 800 °C. Only the βTi interphase boundary was observed in the diffusion couples equilibrated at 1000 and 1100 °C. These experimental data are denoted by the black circles in Fig. 2(c). The open circles in Fig. 2(c) show DSC data obtained in the extreme Zn-rich region.

Besides these experimental phase boundaries, the enthalpy values for the $TiZn_3$ and TiZn phases, estimated using first-principle calculations, were adopted in the assessment of this binary system. The calculated results are listed in Table 5. The calculated values denote the formation

Table 3 Lattice Stability Parameters for Sn, Ti, and Zn

Element	Phase	Lattice stability parameters, J/mol	Temperature, °C	Reference
Sn	(αSn)	$^{\circ}G_{Sn}^{(\alpha Sn)} - {}^{\circ}G_{Sn}^{bct} = -1824.701 - 6.154131T - 0.007101T \ln T + 5.12094 \times 10^{-4}T^2 + 1.784447 \times 10^{-6}T^3 - 2544T^{-1}$	$25 < T < 231.97$	
		$^{\circ}G_{Sn}^{(\alpha Sn)} - {}^{\circ}G_{Sn}^{bct} = -11{,}591.586 + 100.852123T - 13.3160285T \ln T + 8.239147 \times 10^{-3}T^2 - 8.38684 \times 10^{-7}T^3 - 1{,}078{,}700T^{-1} + 1.25305 \times 10^{25}T^{-9}$	$231.97 < T < 526.85$	
		$^{\circ}G_{Sn}^{(\alpha Sn)} - {}^{\circ}G_{Sn}^{bct} = -2656.253 + 8.410508T + 1.25305 \times 10^{25}T^{-9}$	$526.85 < T < 2726.85$	
	(βSn)	$^{\circ}G_{Sn}^{(\beta Sn)} - {}^{\circ}H_{Sn}^{bct} = -7238.3 + 98.676984T - 21.5679761T \ln T - 0.009087376T^2$	$25 < T < 231.97$	
		$^{\circ}G_{Sn}^{(\beta Sn)} - {}^{\circ}H_{Sn}^{bct} = 2528.585 + 3.978992T - 8.2590486T \ln T - 0.016814429T^2 + 2.623131 \times 10^{-6}T^3 - 1{,}081{,}244T^{-1} - 1.25305 \times 10^{25}T^{-9}$	$231.97 < T < 526.85$	2
		$^{\circ}G_{Sn}^{(\beta Sn)} - {}^{\circ}H_{Sn}^{bct} = -8253.098 + 138.970603T - 28.4512T \ln T - 1.25305 \times 10^{25}T^{-9}$	$526.85 < T < 2726.85$	
	bcc	$^{\circ}G_{Sn}^{bcc} - {}^{\circ}G_{Sn}^{bct} = 4400 - 6T$	$25 < T < 2726.85$	
	hcp	$^{\circ}G_{Sn}^{hcp} - {}^{\circ}G_{Sn}^{bct} = 3900 - 4.4T$	$25 < T < 2726.85$	
	L	$^{\circ}G_{Sn}^{L} - {}^{\circ}G_{Sn}^{bct} = 7104.38 - 14.089569T + 1.49503 \times 10^{-18}T^7$	$25 < T < 231.97$	
		$^{\circ}G_{Sn}^{L} - {}^{\circ}G_{Sn}^{bct} = 6970.584 - 13.811447T + 1.25305 \times 10^{25}T^{-9}$	$231.97 < T < 2726.85$	
	$SnTi_3$	$^{\circ}G_{Sn:Sn}^{SnTi_3} - 4 \cdot {}^{\circ}G_{Sn}^{bct} = 0$	$25 < T < 5726.85$	
Ti	bcc	$^{\circ}G_{Ti}^{bcc} - {}^{\circ}H_{Ti}^{hcp} = -1272.064 + 134.78618T - 25.5768T \ln T - 6.63845 \times 10^{-4}T^2 - 2.78803 \times 10^{-7}T^3 + 7208T^{-1}$	$25 < T < 881.85$	2
		$^{\circ}G_{Ti}^{bcc} - {}^{\circ}H_{Ti}^{hcp} = 6667.385 + 105.438379T - 22.3771T \ln T + 0.00121707T^2 - 8.4534 \times 10^{-7}T^3 - 2{,}002{,}750T^{-1}$	$881.85 < T < 1667.85$	
		$^{\circ}G_{Ti}^{bcc} - {}^{\circ}H_{Ti}^{hcp} = 26{,}483.26 - 182.354471T + 19.0900905T \ln T - 0.02200832T^2 + 1.228863 \times 10^{-6}T^3 + 1{,}400{,}501T^{-1}$	$1667.85 < T < 3726.85$	
	bct	$^{\circ}G_{Ti}^{bct} - {}^{\circ}H_{Ti}^{hcp} = 0.01$	$25 < T < 5726.85$	
	hcp	$^{\circ}G_{Ti}^{hcp} - {}^{\circ}H_{Ti}^{hcp} = -8059.921 + 133.687208T - 23.9933T \ln T - 0.004777975T^2 + 1.06716 \times 10^{-7}T^3 + 72{,}636T^{-1}$	$25 < T < 626.85$	
		$^{\circ}G_{Ti}^{hcp} - {}^{\circ}H_{Ti}^{hcp} = -7811.815 + 133.060068T - 23.9887T \ln T - 0.0042033T^2 - 9.0876 \times 10^{-8}T^3 + 42{,}680T^{-1}$	$626.85 < T < 881.85$	2
		$^{\circ}G_{Ti}^{hcp} - {}^{\circ}H_{Ti}^{hcp} = 908.837 + 67.048538T - 14.9466T \ln T - 0.0081465T^2 + 2.02715 \times 10^{-7}T^3 - 1{,}477{,}660T^{-1}$	$881.85 < T < 1667.85$	
		$^{\circ}G_{Ti}^{hcp} - {}^{\circ}H_{Ti}^{hcp} = -124{,}526.786 + 638.878871T - 87.2182461T \ln T + 0.008204849T^2 - 3.04747 \times 10^{-7}T^3 + 36{,}699{,}805T^{-1}$	$1667.85 < T < 3726.85$	
	L	$^{\circ}G_{Ti}^{L} - {}^{\circ}H_{Ti}^{hcp} = 4134.494 + 126.7062T - 23.9933T \ln T - 0.004777975T^2 + 1.06716 \times 10^{-7}T^3 + 72636T^{-1}$	$25 < T < 626.85$	
		$^{\circ}G_{Ti}^{L} - {}^{\circ}H_{Ti}^{hcp} = 4382.601 + 126.0791T - 23.9887T \ln T - 0.0042033T^2 - 9.0876 \times 10^{-8}T^3 + 42680T^{-1}$	$626.85 < T < 881.85$	
		$^{\circ}G_{Ti}^{L} - {}^{\circ}H_{Ti}^{hcp} = 13{,}103.253 + 60.0676T - 14.9466T \ln T - 0.0081465T^2 + 2.02715 \times 10^{-7}T^3 - 1{,}477{,}660T^{-1}$	$881.85 < T < 1026.85$	
		$^{\circ}G_{Ti}^{L} - {}^{\circ}H_{Ti}^{hcp} = 369{,}519.198 - 2553.9505T + 342.059267T \ln T - 0.163409355T^2 + 1.2457117 \times 10^{-5}T^3 - 67{,}034{,}516T^{-1}$	$1026.85 < T < 1667.85$	
		$^{\circ}G_{Ti}^{L} - {}^{\circ}H_{Ti}^{hcp} = -19{,}887.066 + 298.808T - 46.29T \ln T$	$1667.85 < T < 3726.85$	
	$SnTi_3$	$^{\circ}G_{Ti:Ti}^{SnTi_3} - 4 \cdot {}^{\circ}G_{Ti}^{hcp} = 0$	$25 < T < 5726.85$	
Zn	bcc	$^{\circ}G_{Zn}^{bcc} - {}^{\circ}G_{Zn}^{hcp} = 2886.96 - 2.5104T$	$25 < T < 2726.85$	2
	bct	$^{\circ}G_{Zn}^{bct} - {}^{\circ}G_{Zn}^{hcp} = 10{,}000$	$25 < T < 2726.85$	7
	hcp	$^{\circ}G_{Zn}^{hcp} - {}^{\circ}H_{Zn}^{hcp} = -7285.787 + 118.469269T - 23.701314T \ln T - 0.0017120034T^2 - 1.264963 \times 10^{-6}T^3$	$25 < T < 419.58$	2
		$^{\circ}G_{Zn}^{hcp} - {}^{\circ}H_{Zn}^{hcp} = -11{,}070.597 + 172.344911T - 31.38T \ln T + 4.70657 \times 10^{26}T^{-9}$	$419.58 < T < 2726.85$	
	L	$^{\circ}G_{Zn}^{L} - {}^{\circ}G_{Zn}^{hcp} = 7157.27 - 10.292343T - 3.58652 \times 10^{-19}T^7$	$25 < T < 419.58$	2
		$^{\circ}G_{Zn}^{L} - {}^{\circ}G_{Zn}^{hcp} = 7450.123 - 10.736234T - 4.70657 \times 10^{26}T^{-9}$	$419.58 < T < 2726.85$	

enthalpies based on the stable structure of the pure element in the ground state. The entropy terms of the formation energies were estimated from the experimental phase boundaries.

Our thermodynamic description of the Ti-Zn binary system is shown in Table 4. The calculated binary phase diagram is represented by the solid lines in Fig. 2(c). The gas phase, taking part in the equilibrium at higher temperatures caused by the volatilization of the Zn, was treated as an ideal solution of Ti, Ti_2, and Zn. However, at temperatures above 1200 °C, the dominant species in the gas phase was Zn, and this is very stable compared with the βTi or liquid phases. Thus, the solubility of Ti in the gas phase equilibrate with βTi or liquid is restricted, and consequently, it yields an inconsistency in the equilibria at higher temperatures.

Table 4 Thermodynamic parameters of the Sn-Ti-Zn system

System	Phase	Thermodynamic parameters, J/mol	Reference
Sn–Zn	(βSn)	$L^{\beta Sn}_{Sn,Zn} = 9260$	7
	bcc	$L^{bcc}_{Sn,Zn} = 7000$	
	hcp	$L^{hcp}_{Sn,Zn} = 40{,}000$	
	L	$L^{L}_{Sn,Zn} = 12{,}700 - 9.16T + (x_{Sn} - x_{Zn}) \cdot (-5400 + 3.45T) + (x_{Sn} - x_{Zn})^2 \cdot 840$	
Sn–Ti	bcc	$L^{bcc}_{Sn,Ti} = -115{,}000 + 6.77583T + (x_{Sn} - x_{Ti}) \cdot (45{,}000 + 1.58018T)$	4
	bct	$L^{bct}_{Sn,Ti} = 50{,}000$	
	hcp	$L^{hcp}_{Sn,Ti} = -111{,}502.08 + 1.8068T + (x_{Sn} - x_{Ti}) \cdot (43{,}871.41 + 2.08175T)$	
	L	$L^{L}_{Sn,Ti} = -90{,}206.13 - 5.55089T + (x_{Sn} - x_{Ti}) \cdot (44{,}395.59 - 6.09746T)$	
	$SnTi_2$	$^{\circ}G^{SnTi_2}_{Sn,Ti} - {}^{\circ}G^{L}_{Sn} - 2\cdot{}^{\circ}G^{L}_{Ti} = -152{,}700 + 26.80539T$	
	$SnTi_3$	$^{\circ}G^{SnTi_3}_{Ti:Sn} - {}^{\circ}G^{L}_{Sn} - 3\cdot{}^{\circ}G^{L}_{Ti} = -193{,}466.8 + 35.74052T$	
		$^{\circ}G^{SnTi_3}_{Sn:Ti} - 3\cdot{}^{\circ}G^{L}_{Sn} - {}^{\circ}G^{L}_{Ti} = 300{,}000 - 200T$	
		$G^{SnTi_3}_{Sn:Sn,Ti} = 400{,}000$	
		$G^{SnTi_3}_{Ti:Sn,Ti} = 200{,}000 - 108T$	
		$G^{SnTi_3}_{Sn,Ti:Sn} = 400{,}000 - 40T$	
		$G^{SnTi_3}_{Sn,Ti:Ti} = 600{,}000 + 40T$	
	Sn_3Ti_5	$^{\circ}G^{Sn_3Ti_5}_{Sn:Ti} - 3\cdot{}^{\circ}G^{L}_{Sn} - 5\cdot{}^{\circ}G^{L}_{Ti} = -398{,}000 + 64.8T$	
	Sn_5Ti_6	$^{\circ}G^{Sn_5Ti_6}_{Sn:Ti} - 5\cdot{}^{\circ}G^{L}_{Sn} - 6\cdot{}^{\circ}G^{L}_{Ti} = -525{,}800 + 77T$	
Ti–Zn	bcc	$L^{bcc}_{Ti,Zn} = -52{,}000 + 34T$	This work
	hcp	$L^{hcp}_{Ti,Zn} = 32{,}770$	
	Ti_2Zn	$^{\circ}G^{Ti_2Zn}_{Ti:Zn} - 2\cdot{}^{\circ}G^{hcp}_{Ti} - {}^{\circ}G^{hcp}_{Zn} = -54{,}000 + 22.4T$	
	TiZn	$^{\circ}G^{TiZn}_{Ti:Zn} - {}^{\circ}G^{hcp}_{Ti} - {}^{\circ}G^{hcp}_{Zn} = -50{,}800 + 22.5T$	
	$TiZn_2$	$^{\circ}G^{TiZn_2}_{Ti:Zn} - {}^{\circ}G^{hcp}_{Ti} - 2\cdot{}^{\circ}\ G^{hcp}_{Zn} = -80{,}000 + 35.4T$	
	$TiZn_3$	$^{\circ}G^{TiZn_3}_{Ti:Zn} - {}^{\circ}G^{hcp}_{Ti} - 3\cdot{}^{\circ}G^{hcp}_{Zn} = -108{,}000 + 54.6T$	
	$TiZn_5$	$^{\circ}G^{TiZn_5}_{Ti:Zn} - {}^{\circ}G^{hcp}_{Ti} - 5\cdot{}^{\circ}G^{hcp}_{Zn} = -108{,}000 + 51.8T$	
	$TiZn_{10}$	$^{\circ}G^{TiZn_{10}}_{Ti:Zn} - {}^{\circ}G^{hcp}_{Ti} - 10\cdot{}^{\circ}G^{hcp}_{Zn} = -108{,}050 + 47T$	
	$TiZn_{15}$	$^{\circ}G^{TiZn_{15}}_{Ti:Zn} - {}^{\circ}G^{hcp}_{Ti} - 15\cdot{}^{\circ}G^{hcp}_{Zn} = -108{,}100 + 44T$	
	L	$L^{L}_{Ti,Zn} = -30{,}000 + 17.2T$	
Sn–Ti–Zn	$Sn_3Ti_5Zn_{12}$	$^{\circ}G^{Sn_3Ti_5Zn_{12}}_{Sn:Ti:Zn} - 0.15\cdot{}^{\circ}G^{bct}_{Sn} - 0.25\cdot{}^{\circ}\ G^{hcp}_{Ti} - 0.6\cdot{}^{\circ}\ G^{hcp}_{Zn} = -20{,}600$	This work
	L	$L^{L}_{Sn,Ti,Zn} = x_{Sn} \cdot (-16{,}850) + x_{Zn} \cdot (-19{,}350)$	

3.2 Thermodynamic Description of the Sn-Ti-Zn Ternary System

The results of our microstructural analysis using EPMA are summarized in Table 2. The ternary compound formed in samples E6-3, E6-4, and E6-5 equilibrated at 600 °C, as well as in all the samples equilibrated at 700 °C. The chemical composition of the precipitates was close to $Sn_3Ti_5Zn_{12}$. The microstructure of a sample E7-1 at 700 °C observed using optical microscopy is shown in Fig. 4. The ternary compound phase can be seen in the angular crystal grains precipitated in the liquid phase. Determination of the crystal structure was not attempted in the current study. The formation energy of the $Sn_3Ti_5Zn_{12}$ phase was estimated to be −20,600 J/mol to satisfy the observed experimental phase boundaries. The calculated isothermal section diagram at 600 and 700 °C are shown in Fig. 5(a) and (b), respectively. The black circles in Fig. 5(a) and (b) denote samples exhibiting a two-phase structure, and three-phase samples are denoted by triangles.

Figures 6(a)-(c) show the DSC experimental results in the calculated isopleths at 10 mass% Zn, 3 mass% Ti, and 10 mass% Ti, respectively. The experimental peaks in the thermal analysis corresponded to the liquidus lines shown in Fig. 7 in the case of Sn-4mass%Ti-10mass%Zn. However, these were too weak to identify accurately the liquidus temperatures. On the other hand, the peaks of the invariant reactions involving the solid phases were plainly visible, and therefore, the thermodynamic parameter for the liquid phase was determined using the invariant temperatures. The thermodynamic parameters of the ternary system are listed in Table 4.

The calculation of the liquidus projection shown in Fig. 8 reveals that this system includes seven ternary invariant reactions in the Sn-rich region: four peritectic reactions, two remelting, and one ternary eutectic reaction. The ternary eutectic point falls at the 0.0009 mass% Ti, 8.69 mass% Zn composition at $T = 192.40$ °C. These are summarized in Table 6.

3.3 Calculation of the Surface Tension of Liquid Phase

The thermodynamic properties of the Sn-Ti-Zn system determined in this study enabled us to calculate the surface tension of the liquid phase, using the procedure of Speiser and coworkers.[11,12] This is based on Butler's equation,[13] modeling the activity coefficients of a hypothetical surface phase. Equation 8 expresses the surface tension γ of the Sn-Ti-Zn liquid phase:

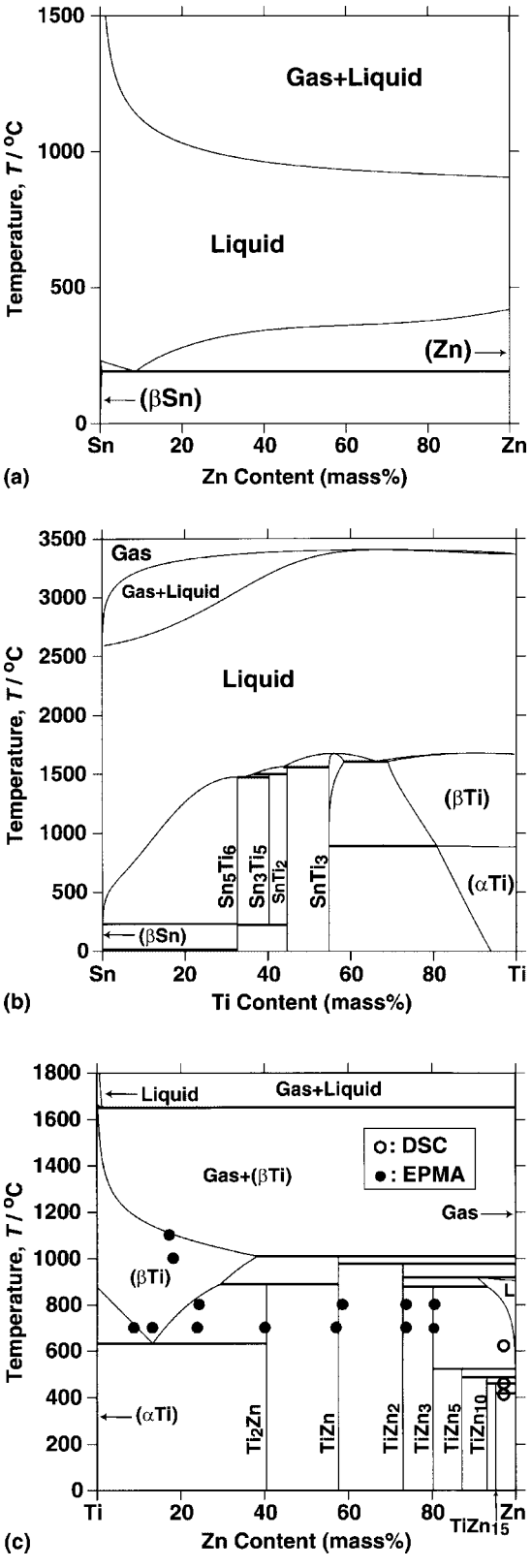

Fig. 2 Calculated phase diagram for (a) the Sn-Zn, (b) the Sn-Ti, and (c) the Ti-Zn binary systems. A comparison of the calculated phase boundaries with the experimental data was carried out in the Ti-Zn phase diagram.

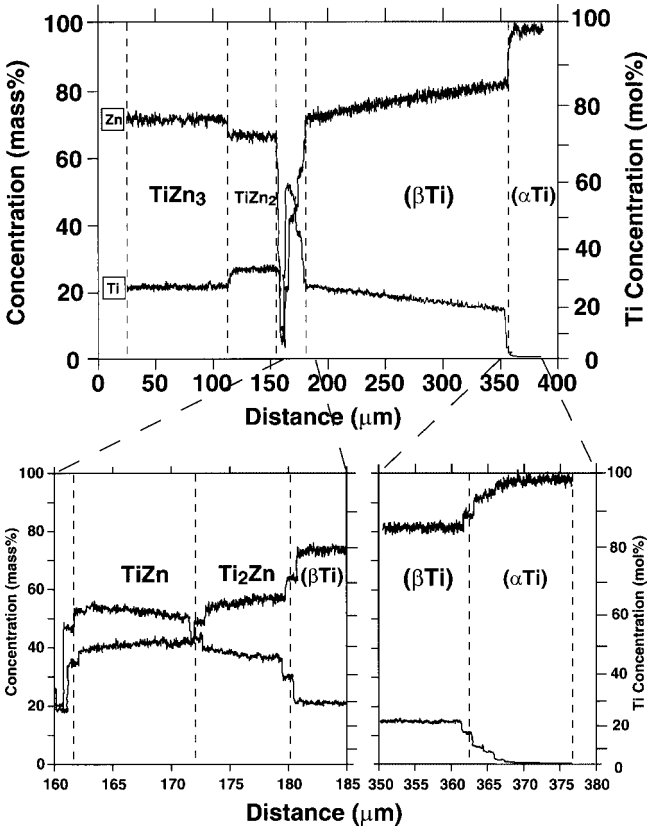

Fig. 3 Concentration profile of the solid-liquid diffusion couple of the Ti-Zn system treated at 700 °C

Table 5 Calculated enthalpy of formation of the $TiZn_3$ and TiZn phases, estimated using first-principle calculations

Phase	Strukturbericht symbol	Space group	Enthalpy of formation (ΔH), J/mol of atoms
$TiZn_3$	$L1_2$	$Pm\bar{3}m$	–27,000
TiZn	B2	$Pm\bar{3}m$	–25,400

$$\gamma = \gamma_{Sn} + \frac{RT}{S_{Sn}} \ln\left(\frac{1 - x_{Ti}^{S} - x_{Zn}^{S}}{1 - x_{Ti}^{B} - x_{Zn}^{B}}\right) + \frac{1}{S_{Sn}}\{\overline{G}_{Sn}^{Ex,S}(T, x_{Ti}^{S}, x_{Zn}^{S}) - \overline{G}_{Sn}^{Ex,B}(T, x_{Ti}^{B}, x_{Zn}^{B})\}$$

$$= \gamma_{Ti} + \frac{RT}{S_{Ti}} \ln\left(\frac{x_{Ti}^{S}}{x_{Ti}^{B}}\right) + \frac{1}{S_{Ti}}\{\overline{G}_{Ti}^{Ex,S}(T, x_{Ti}^{S}, x_{Zn}^{S}) - \overline{G}_{Ti}^{Ex,B}(T, x_{Ti}^{B}, x_{Zn}^{B})\}$$

$$= \gamma_{Zn} + \frac{RT}{S_{Zn}} \ln\left(\frac{x_{Zn}^{S}}{x_{Zn}^{B}}\right) + \frac{1}{S_{Zn}}\{\overline{G}_{Zn}^{Ex,S}(T, x_{Ti}^{S}, x_{Zn}^{S}) - \overline{G}_{Zn}^{Ex,B}(T, x_{Ti}^{B}, x_{Zn}^{B})\} \quad \text{(Eq 8)}$$

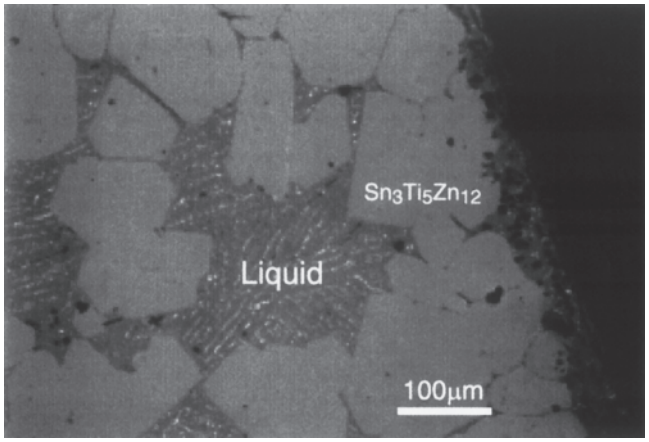

Fig. 4 SEM micrograph of the Sn-9mass%Ti-75mass%Zn alloy (Sample E7-1) equilibrated at 700 °C

where γ_X and S_X denote the surface tension and surface area in a monolayer of a pure liquid X, respectively. S_X can be obtained from the following equation:

$$S_X = L \cdot N_0^{1/3} \cdot V_X^{2/3} \quad \text{(Eq 9)}$$

In Eq 9, N_0 is Avogadro's number, and V_X is the molar volume of a pure liquid X. The value of L in Eq 9 was set to 1.091 for liquid metals, assuming a close packed structure existed. The terms x_X^S and x_X^B denote the mole fractions of component X in the surface phase and bulk phase, respectively. The terms $\overline{G}_X^{Ex,S}$ and $\overline{G}_X^{Ex,B}$ are the partial excess Gibbs energies of component X in the surface phase and the bulk phase, respectively. Equation 10 is assumed to hold between these two properties[14]:

$$\overline{G}^{Ex,S}(T,x_{Ti}^S,x_{Zn}^S) = \beta^{mix} \cdot \overline{G}^{Ex,B}(T,x_{Ti}^S,x_{Zn}^S) \quad \text{(Eq 10)}$$

where β^{mix} is a parameter corresponding to the ratio of the coordination number Z in the surface phase to that in the bulk phase; i.e., Z^S/Z^B. In the current study, β^{mix} was set to 0.75, assuming a close packed structure existed.[11,12] The values for V_X and γ_X in Eq 8 at 450 °C were calculated:

$$V_X = V_{m,X}\{1 + \alpha_X \times (T - T_{m,X})\} \quad \text{(Eq 11)}$$

$$\gamma_X = \gamma_{m,X} + \frac{d\gamma_{m,X}}{dT} \times (T - T_{m,X}) \quad \text{(Eq 12)}$$

where $V_{m,X}$ denotes the liquid atomic volume, $\alpha_{m,X}$ is the thermal coefficient of expansion, $\gamma_{m,X}$ is the surface tension, and $d\gamma_{m,X}/dT$ is the temperature coefficient of the surface tension at the melting temperature $T_{m,X}$ for the pure element X. These values are listed in Table 7,[14] along with the calculated values of V_X and γ_X.

Figure 9 shows the calculated surface tension of Sn-rich Sn-Ti-Zn liquid alloys at 450 °C. These values are slightly higher than those of the conventional Pb-Sn eutectic alloys.[15] Prediction of this type of information is expected to be useful for assessing the feasibility of Pb-free solders.

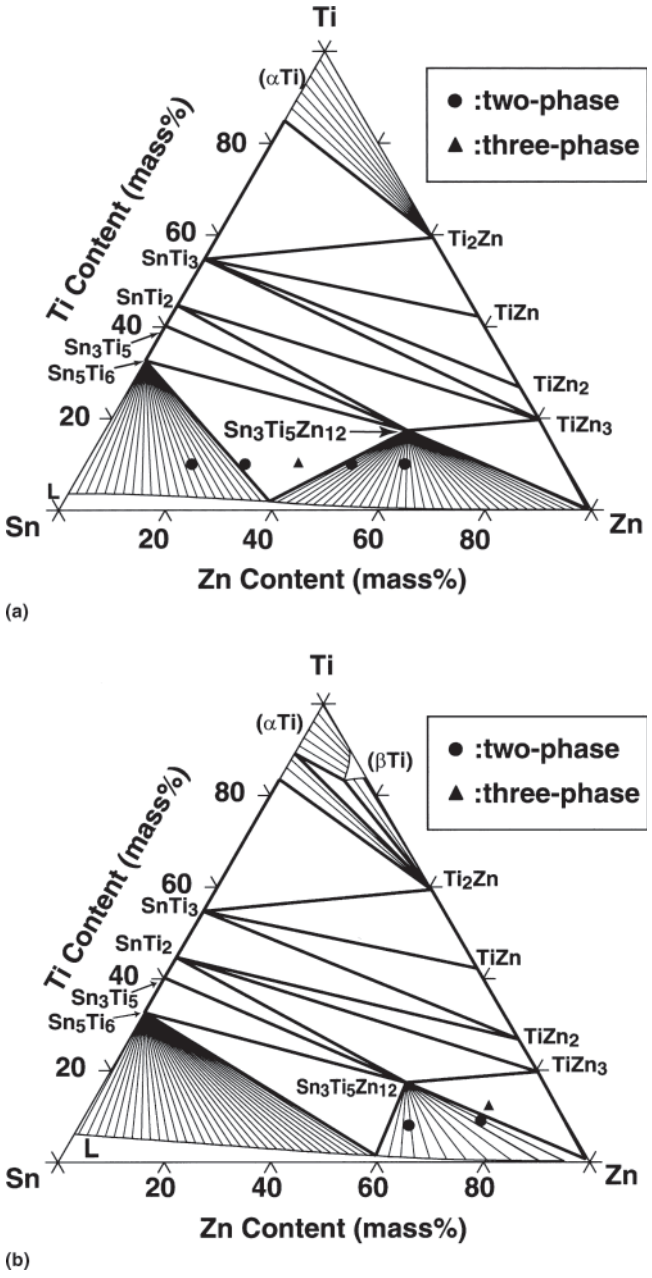

Fig. 5 Calculated phase diagram of the Sn-Ti-Zn ternary system at (a) 600 °C and (b) 700 °C

3.4 Solidification Process Examined using the Scheil Model

The change in concentration of the elements in the liquid phase during the solidification process was calculated using the thermodynamic parameters obtained in our analysis. In our simulations, the so-called Scheil model[16] was used, in which the liquid phase is supercooled several degrees below the equilibrium liquidus temperature in each calculation

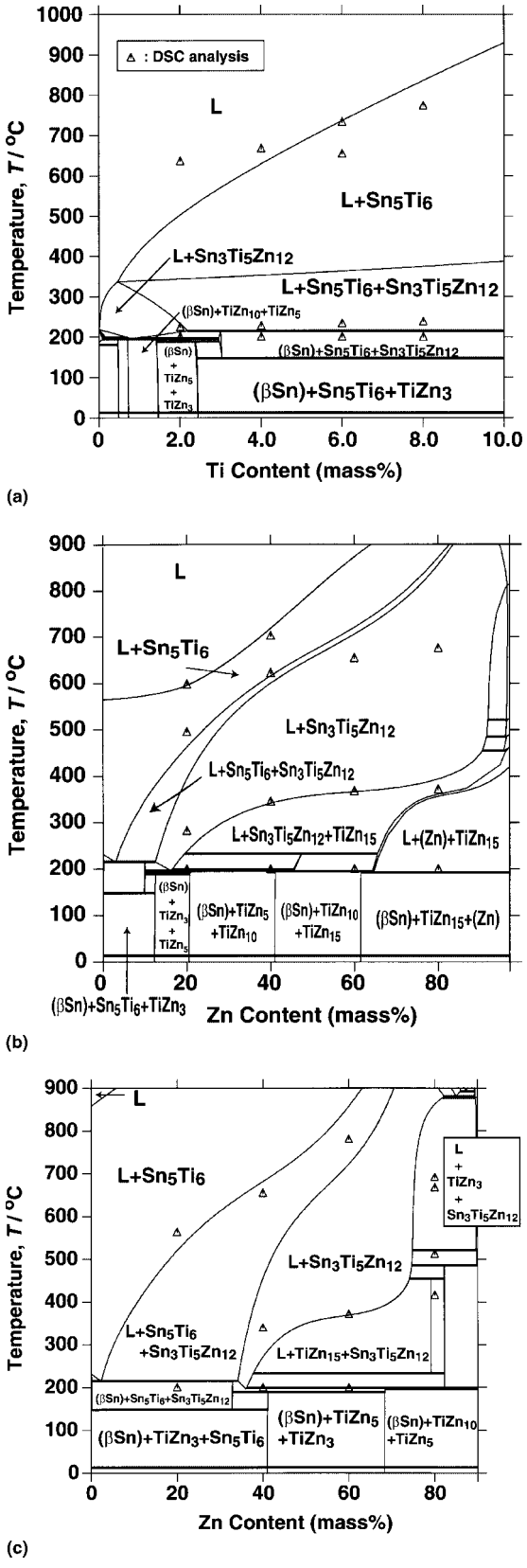

Fig. 6 Comparison of the calculated isopleths with the experimental data at the section of (a) Sn-Ti-10mass%Zn, (b) Sn-3mass%Ti-Zn, and (c) Sn-10mass%Ti-Zn

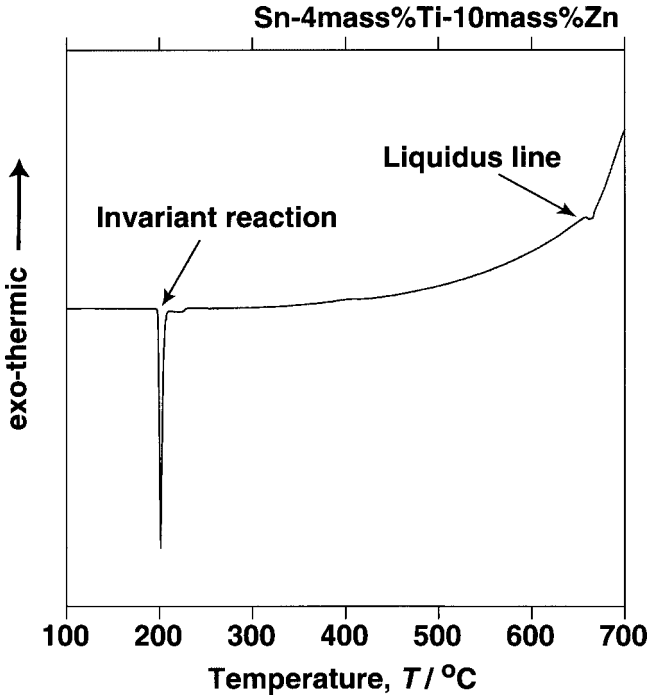

Fig. 7 DSC curve of the Sn-4mass%Ti-10mass%Znalloy

step. The Scheil model assumes that the atoms do not diffuse in the solid phase, and that uniform solidification occurs over the entire liquid range; i.e., that the concentration of each element equilibrates instantaneously. Under such assumptions, the concentration of the diffused element in the solid phase is represented as:

$$C_S = kC_0(1 - f_S)^{k-1} \quad \text{(Eq 13)}$$

where C_0 denotes the content of the original liquid. The equilibrium distribution coefficient between the liquid and solid k is assumed to be constant during solidification. The variable f_s represents the fraction of solid present. The cooling speed is not parameterized in this model. However, it is thought to have been in the middle of the cooling rate between the equilibrium solidification and practical solidification speeds.

Figure 10 shows the calculated results for the Sn-0.005Ti-2Zn (mass%) alloy. The short dashed lines and solid lines denote the calculations of the equilibrium and nonequilibrium solidification processes, respectively. The vertical and horizontal axes show the temperature and the fraction of the solid phase, respectively. The solidification begins at 221.9 °C and ends at 192.4 °C in both processes, and differences in the solidification process between the two cases seem to be quite small. This feature is attributed to the fact that enrichment of each element relative to the liquid phase was prevented owing to the small fraction of precipitates. For example, the phase fraction of the $TiZn_5$ phase crystallized from the liquid phase was calculated to be 0.031%. The narrowness of the solidification range is also the cause of this behavior. A change in the concentration during nonequilibrium solidification is plotted in the liq-

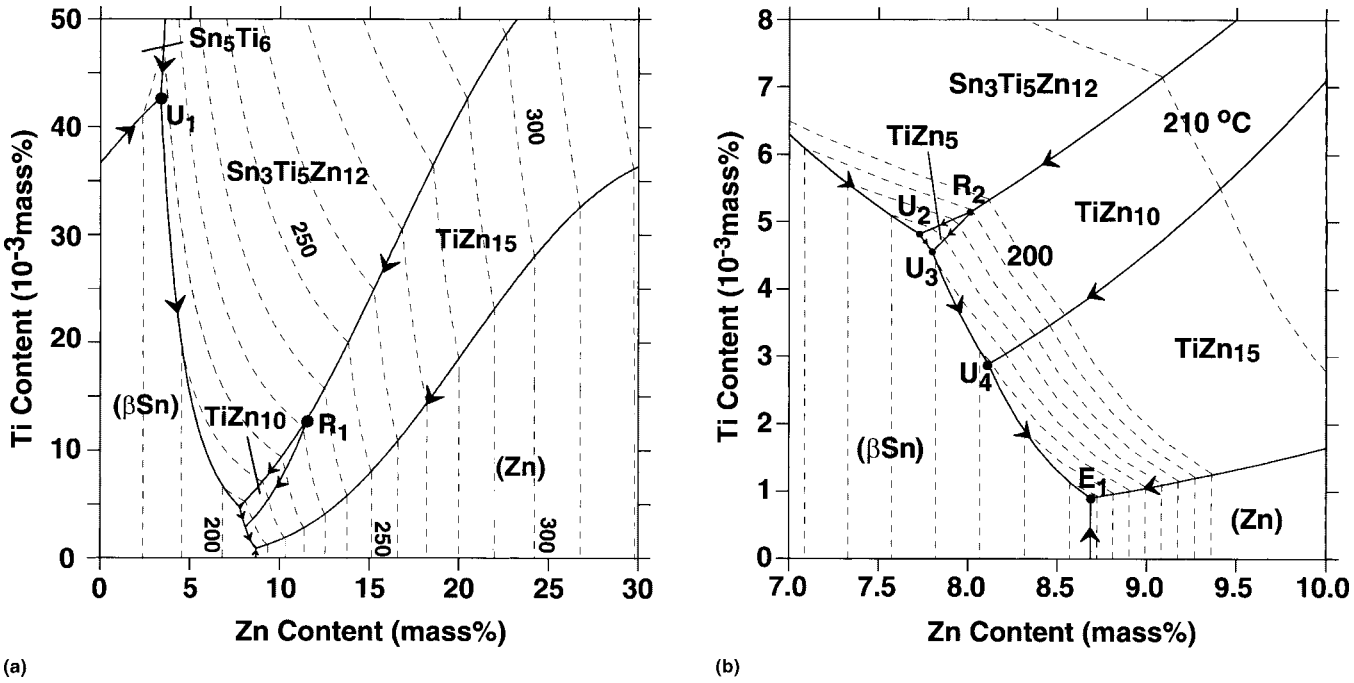

Fig. 8 (a) Sn-rich portion of the calculated liquidus projection of the Sn-Ti-Zn ternary system and (b) an enlarged section

Table 6 Invariant equilibrium reactions related to the Sn-rich liquid phase

			Composition of liquid phase, mass%	
Type	Reaction	Temperature, °C	Ti	Zn
R_1	$TiZn_{15} + Sn_3Ti_5Zn_{12} \rightarrow L + TiZn_{10}$	232.7	0.0132	11.65
R_2	$TiZn_{10} + Sn_3Ti_5Zn_{12} \rightarrow L + TiZn_5$	198.8	0.0052	8.02
U_1	$L + Sn_5Ti_6 \rightarrow Sn_3Ti_5Zn_{12} + (\beta Sn)$	215.2	0.0427	3.36
U_2	$L + Sn_3Ti_5Zn_{12} \rightarrow TiZn_5 + (\beta Sn)$	196.2	0.0048	7.73
U_3	$L + TiZn_5 \rightarrow TiZn_{10} + (\beta Sn)$	195.9	0.0046	7.80
U_4	$L + TiZn_{10} \rightarrow TiZn_{15} + (\beta Sn)$	194.7	0.0029	8.11
E_1	$L \rightarrow (\beta Sn) + (Zn) + TiZn_{15}$	192.4	0.0009	8.69

Table 7 Surface tension and molar volume of pure elements

Elements	$T_{m,X}$, K	$V_{m,X}$, 10^{-6} m^3/mol	α_X, 10^{-4} K^{-1}	V_X at 723 K, 10^{-6} m^3/mol	$\gamma_{m,X}$, mN/m	$d\gamma_X/dT$, mN/m K	γ_X at 723 K, mN/m
Sn	505	17.0	0.87	17.32	561	–0.103	538.55
Ti	1998	11.6	0.56	10.77	1650	–0.26	1981.5
Zn	693	9.94	1.5	9.98	789	–0.21	782.7

uidus projection in Fig. 11. The liquid phase changes composition along the monovariant reaction line as the solidification progresses. The solidification is complete at the ternary eutectic point E_1 while passing through points U_2, U_3, and U_4.

4. Conclusions

A thermodynamic analysis of the Sn-Ti-Zn ternary system was carried out by conducting experimental studies on the phase boundaries using a DSC and by performing EPMA analysis on solid-liquid diffusion couples. The Gibbs energy of the individual phases was expressed using the conventional regular solution approximation. The sublattice model was applied to the $SnTi_3$ phase. The binary intermetallic compound phases with zero homogeneity ranges were treated as being stoichiometric compounds. The results were as follows.

In the thermodynamic description of the Sn-Zn and Sn-Ti binary systems, the results of previous evaluations were adopted. The phase equilibria of the Ti-Zn binary system is

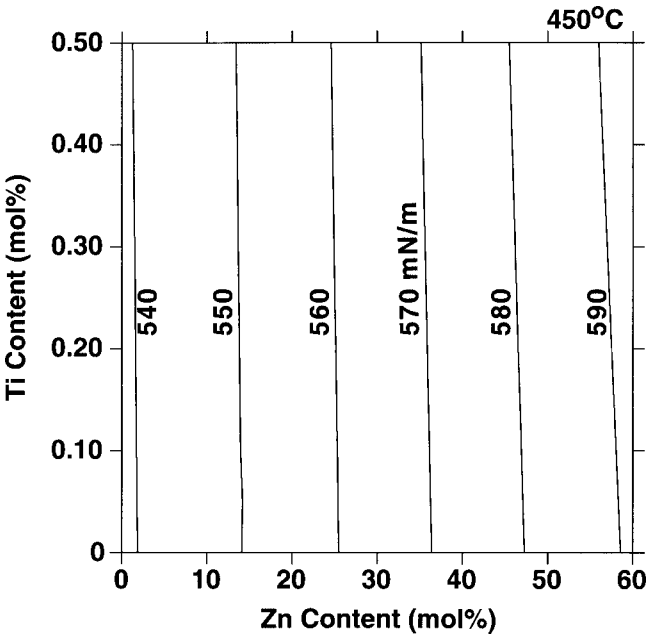

Fig. 9 Calculated surface tension of the Sn-Ti-Zn ternary system at 450 °C

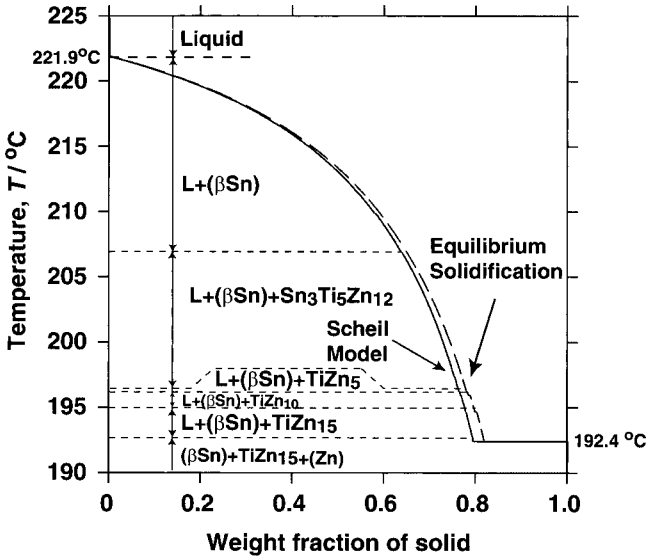

Fig. 10 Calculated nonequilibrium solidification process for the Sn-0.005mass%Ti-2mass%Zn alloy

not well established, and thus, the thermodynamic assessment of the system was performed based on the phase boundaries determined using differential scanning calorimetry as well as the diffusion couples method. In addition, the formation energy of the $TiZn_3$ and TiZn phases was evaluated using first-principle calculations.

Microstructural observations showed that $Sn_3Ti_5Zn_{12}$ exists in the ternary system. The formation energy of this compound and the ternary interaction parameters for the liquid phase were determined from experimental data on the phase boundaries and phase fields. Seven types of invariant

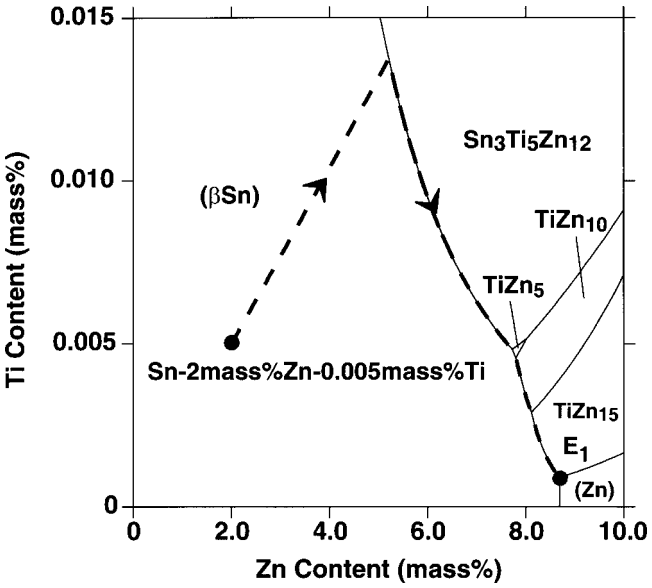

Fig. 11 Nonequilibrium solidification path of the Sn-0.005mass%Ti-2mass%Zn alloy plotted in the liquidus projection

reaction on the Sn-rich liquidus surface of the ternary system were predicted by the phase diagram calculations. The ternary eutectic point falls at the 0.0009 mass% Ti, 8.69 mass% Zn composition at $T = 192.40$ °C.

Based on these results, a nonequilibrium solidification process using the Scheil model was simulated. The behavior was not much different from that of the equilibrium solidification process. This feature is attributed to the low enrichment of each element relative to the liquid phase, as well as narrowness of the solidification range. The calculated surface tension of the liquid phase based on Butler's equation was slightly higher than that of conventional Pb-Sn eutectic alloys.

Acknowledgments

The authors gratefully acknowledge the experimental support of Mr. Shiraishi and Ms. Kinoshita at the Kyushu Institute of Technology, Japan. This work was partially supported by a Grant-in-aid for Scientific Research (No. 14550720) from the Ministry of Education, Science, Sports and Culture of Japan.

References

1. T. Takemoto, Lead-free Solder and Micro-joining, *Materia Jpn.,* 1996, 35, p 320-325 (in Japanese)
2. A.T. Dinsdale, SGTE Data for Pure Elements, *CALPHAD,* 1991, 15, p 317-425
3. O. Redlich and A.T. Kister, Algebraic Representation of Thermodynamic Properties and the Classification of Solutions, *Ind. Eng. Chem.,* 1948, 40, p 354-384
4. F. Hayes, Thermodynamic Database for Light Metal Alloys, *COST 507,* Volume 2, I. Ansara, A.T. Dinsdale, and M.H. Rand, Ed., Office for Official Publications of the European Communities, Luxembourg, 1998, p 284-287
5. P. Blaha, K. Schwarz, G.K.H. Madsen, D. Kvasnicka, and J.

Luitz, *WIEN2k: An Augmented Plane Wave + Local Orbitals Program for Calculating Crystal Properties,* Karlheinz Schwarz, Techn. Universität Wien, Austria, 2001.
6. J.P. Perdew, K. Burke, and Y. Wang, Generalized Gradient Approximation for the Exchange-Correlation Hole of a Many-Electron System, *Phys. Rev. B,* 1996, 54, p 16533-16539
7. H. Ohtani, M. Miyashita, and K. Ishida, Thermodynamic Study of Phase Equilibria in the Sn-Ag-Zn System, *J. Jpn. Inst. Metals,* 1999, 63(6), p 685-694
8. *Phase Diagram of Binary Titanium Alloys,* J.L. Murray, Ed., ASM International, Metals Park, OH, 1987, p 340-345
9. G.P. Vassilev, X.J. Liu, and K. Ishida, Reaction Kinetics and Phase Diagram Studies in the Ti-Zn System, *J. Alloys Compd.,* 2004, 375, p 162-170
10. G.P. Vassilev, Contribution to the Zinc-Rich Side of the Ti-Zn System, *Z. Metallkde.,* 2004, 95(9), p 813-817
11. R. Speiser, D.R. Poirier, and K. Yeum, Surface Tension of Binary Liquid Alloys, *Scripta Metall.,* 1987, 21(5), p 687-692
12. K.S. Yeum, R. Speiser, and D.R. Poirier, Estimation of the Surface Tensions of Binary Liquid Alloys, *Metall. Trans. B,* 1989, 20, p 693-703
13. J.A.V. Butler, The Thermodynamics of the Surface of Solutions, *Proc. R. Soc.,* 1932, 135, p 348-375
14. T. Tanaka and T. Iida, Application of a Thermodynamic Database to the Calculation of Surface Tension for Iron-Base Liquid Alloys, *Steel Res.,* 1994, 65, p 21-27
15. T.P. Hoar and D.A. Melford, The Surface Tension of Binary Liquid Mixtures, Lead + Tin and Lead + Indium Alloys, *Trans. Faraday Soc.,* 1957, 53, p 315-326
16. E. Scheil, Comments on Crystallization, *Z. Metallkde.,* 1942, 34, p 70-72 (in German)